

Production of Λ_c^+ hypernuclei in antiproton - nucleus collisions

R. Shyam^a, K. Tsushima^b

^a*Saha Institute of Nuclear Physics, 1/AF Bidhan Nagar, Kolkata 700064, India*

^b*Laboratório de Física Teórica e Computacional, Universidade Cruzeiro do Sul, Rua Galvão Bueno, 868, Liberdade 01506-000, São Paulo, SP, Brazil*

Abstract

We investigate the production of charm-baryon hypernucleus $^{16}_{\Lambda_c^+}\text{O}$ in the antiproton - ^{16}O collisions within a fully covariant model that is based on an effective Lagrangian approach. The explicit $\bar{\Lambda}_c^-\Lambda_c^+$ production vertex is described by the t -channel D^0 and D^{*0} meson-exchanges in the initial collision of the incident antiproton with one of the protons of the target nucleus. The Λ_c^+ bound state spinors as well as the self-energies of the exchanged mesons employed in our calculations are derived from the quark-meson coupling model. The parameters of various vertices are taken to be the same as those used in our previous study of the elementary $\bar{p} + p \rightarrow \bar{\Lambda}_c^- + \Lambda_c^+$ reaction. We find that for antiproton beam momenta of interest to the $\bar{P}ANDA$ experiment, the 0° differential cross sections for the formation of $^{16}_{\Lambda_c^+}\text{O}$ hypernuclear states with simple particle-hole configurations, have magnitudes in the range of a few $\mu\text{b}/\text{sr}$.

Keywords: Production of Λ_c^+ hypernuclei, antiproton-nucleus collisions, covariant production model, bound charm-baryon spinors from quark-meson coupling model

PACS: 14.20.Lq, 11.10.Ef, 12.39.Ki, 13.60.Rj

The investigation of the production of heavy flavor hadrons consisting of a charm-quark is of considerable interest as it provides an additional means for a better understanding of quantum chromodynamics (QCD) (see, e.g., Refs. [1, 2]). The future $\bar{P}ANDA$ ("antiproton annihilation at Darmstadt") experiment at the under-construction antiproton and ion research facility (FAIR) in Darmstadt, Germany, includes a rich program on the measurements of the charm-meson and charm-baryon production in the antiproton

(\bar{p}) collisions with proton and nuclei at the beam momenta ≤ 15 GeV/c [3]. The accurate knowledge of the charm-meson $\bar{D}D$ ($\bar{D}^0 D^0$ and $D^- D^+$) production cross sections in these reactions, is important because the charmonium states above the open charm threshold will generally be identified by means of their decays to $\bar{D}D$ channels if allowed [4, 5].

Studies of the production and spectroscopy of charm-baryons (e.g. Λ_c^+) are similarly interesting. In contrast to the mesons, there can be more states of these systems as there are more possibilities of orbital excitations due the presence of three quarks. At higher \bar{p} beam momenta at the $\bar{P}ANDA$ facility the yields of the channels with charm-baryons exceed those of the charm-meson channels by factors of 3-4, which is confirmed by calculations of the productions of $\bar{\Lambda}_c^- \Lambda_c^+$ and $\bar{D}D$ pairs in the $\bar{p}p$ collisions in Refs. [6, 7, 8, 9]. In studies of the charm-baryon production in the \bar{p} induced reactions on proton or nuclei the production of extra particles is not needed for the charm conservation, which reduces the threshold energy as compared to, say, pp collisions. Investigations of the charm-baryon (and also charm-meson) productions in the \bar{p} -nucleus collisions explore the properties of charm-hadrons in the nuclear medium and provide information about the charm hadron-nucleon (N) interaction in the nuclear medium [10, 11, 12].

The $\Lambda_c^+ - N$ interaction has come in focus after discoveries of many exotic hadrons [e.g. $X(3872)$, and $Z(4430)$] by the Belle experiments [13, 14]. These hadrons are considered to be either the 4-quark bound states including the charm one or the composite states of two (or more) hadrons (see, e.g., Ref. [15] for a review). There is no conclusive evidence for the existence of the two-body bound states in the $\Lambda_c^+ - N$ channel. It will critically depend on the nature of the $\Lambda_c^+ - N$ interaction. Because performing scattering experiments in this channel is not feasible for the time being, alternative methods will have to be explored for determining this interaction. Some effort has been made in this direction in the lattice QCD calculations by the HAL QCD collaboration [16], but their results are limited to pion masses around or in excess of 600 MeV. Another viable alternative is to study Λ_c^+ hypernuclei that can be produced in the \bar{p} induced reactions on nuclei at the $\bar{P}ANDA$ facility. In the past the study of the Λ hypernuclear states has provided important information about the $\Lambda - N$ interaction (see, e.g., the reviews [17, 18, 19]). Furthermore, in a theoretical study of the Ξ -hypernuclei, it has been shown that the properties of the states of such nuclei are strongly dependent on the nature of the $\Xi - N$ interaction [20].

The existence of the Λ_c^+ hypernuclei was predicted already in 1975 [21].

Since then several theoretical calculations have been reported for such nuclei that are based on the idea of the close similarity between the quark structures of Λ and Λ_c^+ . They have predicted a rich spectrum of charm-hypernuclei spanning over a wide range of atomic mass numbers [22, 23, 24, 25, 26, 27, 28, 29]. However, there is a large variation in the binding energies and the potential depths predicted by these authors. More recently, in a series of publications [30, 31, 32, 33] systematic and quantitative studies of the Λ_c^+ hypernuclei have been reported within the quark-meson coupling (QMC) model. These studies have predicted a number of states and their binding energies for the Λ_c^+ hypernuclei, $^{17}_{\Lambda_c^+}\text{O}$, $^{41}_{\Lambda_c^+}\text{Ca}$, $^{49}_{\Lambda_c^+}\text{Ca}$, $^{91}_{\Lambda_c^+}\text{Zr}$, and $^{209}_{\Lambda_c^+}\text{Pb}$. However, none of these references reports any production cross section for the formation of the Λ_c^+ hypernuclei in an actual reaction.

In this letter, we present, for the first time, results for the cross sections of the Λ_c^+ hypernuclear production in the \bar{p} - ^{16}O collisions. We describe this reaction within an effective Lagrangian model (see, e.g. Refs. [20, 34, 35, 36, 37]), where $\bar{\Lambda}_c^-\Lambda_c^+$ production takes place via t -channel exchanges of D^0 and D^{*0} mesons in collisions of the \bar{p} with one of the protons of the target nucleus in the initial state [see, Figs. 1(a) and 1(b)]. The Λ_c^+ is captured into one of the orbits of the residual nucleus to make the hypernucleus, while $\bar{\Lambda}_c^-$ rescatters onto its mass shell [Fig. 1(a)]. The s - and u -channel resonance excitation diagrams are suppressed, as no resonance is known with energy in excess of 3.0 GeV having branching ratios for decay to the Λ_c^+ channel. The direct $\bar{p}p$ annihilation into $\bar{\Lambda}_c^-\Lambda_c^+$ via the contact diagrams is also suppressed due to the Okubo-Zweig-Iizuka rule.

It may be noted that the free space $\bar{\Lambda}_c^-\Lambda_c^+$ productions in the $\bar{p}p$ collisions have been studied in Refs. [8, 38] within the Jülich meson-baryon model in a coupled-channel approach. In these studies, where calculations are confined to antiproton beam momenta lying close to the charm baryon production threshold, the coupled-channel effects have been found to be very important. Even though the role of the coupled-channel effects has not been studied at higher \bar{p} beam momenta of relevance to the $\bar{P}ANDA$ experiment, which are of interest to our work, these effects may not be as strong at such higher beam momenta as they are at near threshold beam momenta. Inclusion of the coupled-channel effects of the kind discussed in Refs. [8, 38] is currently out of the scope of our effective Lagrangian model.

Our model retains the full structure of the interaction vertices and treats baryons as Dirac particles. The Λ_c^+ bound state spinors have been calculated

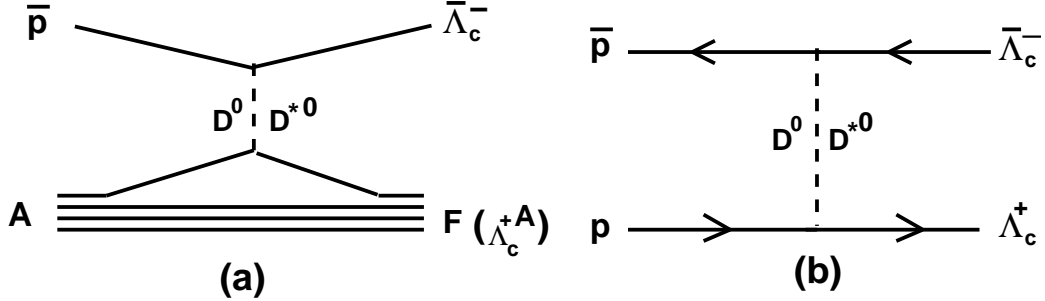


Figure 1: (a) Graphical representation of the model used to describe the charm-hypernuclear production reaction $\bar{p} + A \rightarrow \bar{\Lambda}_c^- + F(= \Lambda_c^+ A)$. D^0 and D^{*0} in the intermediate line represent the exchanges of D^0 pseudoscalar and D^{*0} vector mesons, respectively. (b) The diagram to describe the elementary reaction $\bar{p} + p \rightarrow \bar{\Lambda}_c^- + \Lambda_c^+$. The arrows show the directions of the relative momenta.

within the QMC model. In this model [39], quarks within the non-overlapping nucleon bags (modeled using the MIT bag), interact self-consistently with the isoscalar-scalar (σ) and isoscalar-vector (ω) mesons in the mean field approximation. The explicit treatment of the nucleon internal structure represents an important departure from quantum hadrodynamics (QHD) [40]. The self-consistent response of bound quarks to the mean σ field leads to a new saturation mechanism for nuclear matter [39]. The QMC model has been used to study the properties of finite nuclei [41], the binding of ω , η , η' and D mesic nuclei [42, 43, 44] and also the effect of the medium on K^\pm and J/Ψ production [45].

For the evaluation of the amplitudes corresponding to the processes shown in Fig. 1(a), one requires the effective Lagrangians at the baryon-meson-nucleon vertices, and the propagators for the D^0 and D^{*0} mesons. The masses of these mesons have been taken to be 1.867 GeV and 2.008 GeV, respectively. The denominators of these propagators involve the meson self-energies that account for the medium effects on their propagation through the nucleus.

The effective Lagrangians at the charm-baryon-meson-nucleon vertices have been adopted from Refs. [6, 46, 47, 48]. For the D^0 meson-exchange vertices we have

$$\mathcal{L}_{D^0 BN} = ig_{BD^0 N} \bar{\psi}_B \gamma_5 \psi_N \phi_{D^0} + H.c., \quad (1)$$

where ψ_B and ψ_N are the charm-baryon and nucleon (antinucleon) fields,

respectively, while ϕ_{D^0} is the D^0 meson field. g_{BD^0N} in Eq. (1) represents the vertex coupling constant at the charm-baryon(B)- D^0 -meson-nucleon (-antinucleon) vertex.

For the D^{*0} meson-exchange vertices, the effective Lagrangian is

$$\mathcal{L}_{D^{*0}BN} = g_{D^{*0}BN} \bar{\psi}_B \gamma_\mu \psi_N \theta_{D^{*0}}^\mu + \frac{f_{D^{*0}BN}}{4M} \bar{\psi}_B \sigma_{\mu\nu} \psi_N G_{D^{*0}}^{\mu\nu} + H.c., \quad (2)$$

where $\theta_{D^{*0}}^\mu$ is the vector meson field, with field strength tensor $G_{D^{*0}}^{\mu\nu} = \partial^\mu \theta_{D^{*0}}^\nu - \partial^\nu \theta_{D^{*0}}^\mu$, and $\sigma_{\mu\nu}$ is the usual tensor operator in the Dirac space. The vector and tensor couplings are defined by g and f , respectively.

The values of g and f at various vertices are adopted from Refs. [47, 49, 50], as $g_{ND^0B} = 13.98$, $g_{ND^{*0}B} = 5.64$ and $f_{ND^{*0}B} = 18.37$. We add that the same coupling constants were used in the description of the free-space charmed hadron production in $\bar{p}p$ collisions within the effective Lagrangian model [6, 7] as well as the Jülich meson-exchange model [8, 9, 38]. Furthermore, same values of the vector and tensor couplings were also used in Ref. [48] in investigations of the role of intrinsic charm in the nucleon using a model formulated in terms of effective meson-baryon degrees of freedom.

The off-shell corrections at various vertices are accounted for by introducing form factors (F_i). In our study of the free-space $\bar{\Lambda}_c^- + \Lambda_c^+$ production [6], monopole form factors [51, 52] were used at all the vertices. In order to maintain consistency with these calculations, we employ form factors of the same shape (monopole) to regulate the off-shell behavior of the vertices in the present work. We write

$$F_i(q_{D_i}) = \frac{\lambda_i^2 - m_{D_i}^2}{\lambda_i^2 - q_{D_i}^2}, \quad (3)$$

with a cutoff parameter (λ_i) of 3.0 GeV, which is the same as that used in Ref. [6]. In Eq. 3, q_{D_i} is the momentum of the i -th exchanged meson with mass m_{D_i} . It may be noted that the same shape of the form factor with the same λ_i was also used in the studies of the $\bar{D}D$ production in $\bar{p}p$ and \bar{p} -nucleus collisions in Refs. [7] and [10], respectively, within a similar type of the effective Lagrangian model.

The propagators for the D^0 and D^{*0} mesons are given by

$$G_{D^0}(q_{D^0}) = \frac{i}{q_{D^0}^2 - m_{D^0}^2 - \Pi_{D^0}}, \quad (4)$$

$$G_{D^{*0}}^{\mu\nu}(q_{D^{*0}}) = -i \left(\frac{g^{\mu\nu} - q_{D^{*0}}^\mu q_{D^{*0}}^\nu / q_{D^{*0}}^2}{q_{D^{*0}}^2 - (m_{D^{*0}} - i\Gamma_{D^{*0}}/2)^2 - \Pi_{D^{*0}}} \right), \quad (5)$$

where q_{D^0} and $q_{D^{*0}}$ are the four-momenta of D^0 and D^{*0} mesons, respectively, while m_{D^0} and $m_{D^{*0}}$ are their masses. Π_{D^0} and $\Pi_{D^{*0}}$ represent the (complex) self-energies of D^0 and D^{*0} mesons, respectively. In Eq. (5), $\Gamma_{D^{*0}}$ is the total width of the D^{*0} meson, which is about 2.0 MeV according to the latest particle data group estimate [53].

In this exploratory study, the self-energies Π_{D^0} and $\Pi_{D^{*0}}$ have been obtained from the mean-field potentials for D^0 and D^{*0} mesons in ^{16}O calculated self-consistently within the QMC model in the local density approximation as described in Ref. [44]. The self-energy is related to the potential by $\Pi_{D_i} = 2\omega_{D_i}U_{D_i}(q_{D_i})$, where $\omega_{D_i} = \sqrt{q_{D_i}^2 + m_{D_i}^2}$, and U_{D_i} is the potential in the momentum space of meson D_i , with D_i standing for D^0 or D^{*0} .

After having established the effective Lagrangians, coupling constants, and forms of the propagators, the amplitudes of D^0 and D^{*0} exchange diagrams can be easily written. The signs of these amplitudes are fixed by those of the effective Lagrangians, the coupling constants, and the propagators as described above. These signs are not allowed to change anywhere in the calculations.

At the upper vertices of Fig. 1(a), the amplitudes involve free-space spinors of the antiparticles, while at the lower vertices, they have spinors for bound proton in the initial state (to be represented by $\psi(k_p)$) and bound Λ_c^+ in the final state (to be represented by $\psi(k_{\Lambda_c^+})$). These are the four component Dirac spinors, which are solutions of the Dirac equation for a bound state problem in the presence of external potential fields. They are calculated within the QMC model as described below. We write

$$\psi(k_i) = \delta(k_{i0} - E_i) \begin{pmatrix} f(K_i)\mathcal{Y}_{\ell 1/2 j}^{m_j}(\hat{k}_i) \\ -ig(K_i)\mathcal{Y}_{\ell' 1/2 j}^{m_j}(\hat{k}_i) \end{pmatrix}. \quad (6)$$

In our notation k_i represents a four momentum, and \mathbf{k}_i a three momentum. The magnitude of \mathbf{k}_i is represented by K_i , and its directions by \hat{k}_i . k_{i0} represents the timelike component of momentum k_i . In Eq. (6), $f(K_i)$ and $g(K_i)$ are the radial parts of the upper and lower components of the spinor $\psi(k_i)$ with i representing either a proton or a Λ_c^+ . The coupled spherical harmonics, $\mathcal{Y}_{\ell 1/2 j}^{m_j}$, is given by

$$\mathcal{Y}_{\ell 1/2 j}^{m_j}(\hat{k}_i) = \langle \ell m_\ell 1/2 \mu | j m_j \rangle Y_{\ell m_\ell}(\hat{k}_i) \chi_\mu, \quad (7)$$

where $Y_{\ell m_\ell}$ represents the spherical harmonics, and χ_μ the spin-space wave function of a spin- $\frac{1}{2}$ particle. In Eq. (6) $\ell' = 2j - \ell$ with ℓ and j being the orbital and total angular momenta, respectively.

To calculate the spinors for the final bound charm-hypernuclear state and the initial proton bound state within the QMC model, we construct a simple, relativistic shell model, with the nucleon core calculated in a combination of self-consistent scalar and vector mean fields. The Lagrangian density for a hypernuclear system in the QMC model is written as a sum of two terms,

$$\mathcal{L}_{QMC}^{HY} = \mathcal{L}_{QMC}^N + \mathcal{L}_{QMC}^Y, \quad (8)$$

$$\begin{aligned} \mathcal{L}_{QMC}^N \equiv & \bar{\psi}_N(\mathbf{r}) \left[i\gamma \cdot \partial - M_N^*(\sigma) - (g_\omega \omega(\mathbf{r}) + g_\rho \frac{\tau_3^N}{2} b(\mathbf{r}) + \frac{e}{2}(1 + \tau_3^N) A(\mathbf{r})) \gamma_0 \right] \psi_N(\mathbf{r}) \\ & - \frac{1}{2}[(\nabla \sigma(\mathbf{r}))^2 + m_\sigma^2 \sigma(\mathbf{r})^2] + \frac{1}{2}[(\nabla \omega(\mathbf{r}))^2 + m_\omega^2 \omega(\mathbf{r})^2] \\ & + \frac{1}{2}[(\nabla b(\mathbf{r}))^2 + m_\rho^2 b(\mathbf{r})^2] + \frac{1}{2}(\nabla A(\mathbf{r}))^2, \end{aligned} \quad (9)$$

$$\begin{aligned} \mathcal{L}_{QMC}^Y \equiv & \bar{\psi}_Y(\mathbf{r}) [i\gamma \cdot \partial - M_Y^*(\sigma) - (g_\omega^Y \omega(\mathbf{r}) + g_\rho^Y I_3^Y b(\mathbf{r}) + eQ_Y A(\mathbf{r})) \gamma_0] \psi_Y(\mathbf{r}), \\ & (Y = \Lambda, \Sigma^{0,\pm}, \Xi^{0,+}, \Lambda_c^+, \Sigma_c^{0,+,++}, \Xi_c^{0,+}, \Lambda_b), \end{aligned} \quad (10)$$

where $\psi_N(\mathbf{r})$ and $\psi_Y(\mathbf{r})$ are the nucleon and the hyperon (strange, charm or bottom baryon) fields, respectively. $A(r)$ is the Coulomb field. g_ω and g_ρ are the ω -N and ρ -N coupling constants which are related to the corresponding (u, d) quark- ω , g_ω^q , and (u, d) quark- ρ , g_ρ^q , coupling constants, as $g_\omega = 3g_\omega^q$ and $g_\rho = g_\rho^q$. I_3^Y and Q_Y are the third component of the hyperon isospin operator and its electric charge in units of the proton charge, e , respectively.

The following set of equations of motion are obtained for the hypernuclear system from the Lagrangian densities defined by Eqs. (9)-(10),

$$[i\gamma \cdot \partial - M_N(\sigma) - (g_\omega \omega(\mathbf{r}) + g_\rho \frac{\tau_3^N}{2} b(\mathbf{r}) + \frac{e}{2}(1 + \tau_3^N) A(\mathbf{r})) \gamma_0] \psi_N(\mathbf{r}) = 0, \quad (11)$$

$$[i\gamma \cdot \partial - M_Y(\sigma) - (g_\omega^Y \omega(\mathbf{r}) + g_\rho^Y I_3^Y b(\mathbf{r}) + eQ_Y A(\mathbf{r})) \gamma_0] \psi_Y(\mathbf{r}) = 0, \quad (12)$$

$$(-\nabla_r^2 + m_\sigma^2) \sigma(\mathbf{r}) = g_\sigma C_N(\sigma) \rho_s(\mathbf{r}) + g_\sigma^Y C_Y(\sigma) \rho_s^Y(\mathbf{r}), \quad (13)$$

$$(-\nabla_r^2 + m_\omega^2) \omega(\mathbf{r}) = g_\omega \rho_B(\mathbf{r}) + g_\omega^Y \rho_B^Y(\mathbf{r}), \quad (14)$$

$$(-\nabla_r^2 + m_\rho^2) b(\mathbf{r}) = \frac{g_\rho}{2} \rho_3(\mathbf{r}) + g_\rho^Y I_3^Y \rho_B^Y(\mathbf{r}), \quad (15)$$

$$(-\nabla_r^2) A(\mathbf{r}) = e\rho_p(\mathbf{r}) + eQ_Y \rho_B^Y(\mathbf{r}), \quad (16)$$

where, $\rho_s(\mathbf{r})$ ($\rho_s^Y(\mathbf{r})$), $\rho_B(\mathbf{r})$ ($\rho_B^Y(\mathbf{r})$), $\rho_3(\mathbf{r})$ and $\rho_p(\mathbf{r})$ are the scalar, baryon, third component of isovector, and proton densities at position \mathbf{r} in the hyper-

Table 1: Binding energies of Λ_c^+ and p for each shell as predicted by the QMC model.

State	BE (MeV)
$^{16}_{\Lambda_c^+}\text{O}(\Lambda_c^+ 0p_{1/2})$	7.17
$^{16}_{\Lambda_c^+}\text{O}(\Lambda_c^+ 0p_{3/2})$	7.20
$^{16}_{\Lambda_c^+}\text{O}(\Lambda_c^+ 0s_{1/2})$	12.78
$^{16}\text{O}(p 0p_{1/2})$	11.87

nucleus [42]. On the right hand side of Eq. (13), a new and characteristic feature of the QMC model appears that arises from the internal structures of the nucleon and hyperon, namely, $g_\sigma C_N(\sigma) = -\frac{\partial M_N(\sigma)}{\partial \sigma}$ and $g_\sigma^Y C_Y(\sigma) = -\frac{\partial M_Y(\sigma)}{\partial \sigma}$ where $g_\sigma \equiv g_\sigma(\sigma = 0)$ and $g_\sigma^Y \equiv g_\sigma^Y(\sigma = 0)$. We use the nucleon and hyperon masses to calculate $C_{N,Y}(\sigma)$ employing the parameters of QMC-I summarized in table 13 of Ref. [45]. The scalar and vector fields as well as the spinors for hyperons and nucleons, can be obtained by solving these coupled equations self-consistently.

We note here that, for the Dirac equation for Λ_c^+ baryon [Eq. (12)], the effects of Pauli blocking at the quark level, is introduced by adding a repulsive potential. This is the same as that used for the Λ -hyperon case. This was extracted by the fit to the Λ - and Σ -hypernuclei taking into account the $\Sigma N - \Lambda N$ channel coupling [31, 32, 33, 43]. The modified Dirac equation for the Λ_c^+ baryon is,

$$[i\gamma \cdot \partial - M_Y(\sigma) - (\lambda_{\Lambda_c^+} \rho_B(\mathbf{r}) + g_\omega^Y \omega(\mathbf{r}) + g_\rho I_3^Y b(\mathbf{r}) + eQ_Y A(\mathbf{r}))\gamma_0]\psi_Y(\mathbf{r}) = 0, \quad (17)$$

where $\rho_B(\mathbf{r})$ is the baryon density at the position \mathbf{r} in the Λ_c^+ -hypernucleus. The value of $\lambda_{\Lambda_c^+}$ is 60.25 MeV (fm)³. The details about the effective Pauli blocking at the quark level can be found in Refs. [43, 45].

We have chosen the reaction $\bar{p} + ^{16}\text{O} \rightarrow \bar{\Lambda}_c^- + ^{16}_{\Lambda_c^+}\text{O}$ for the first numerical application of our model of charm-hypernuclear production. The target nucleus is a doubly closed system. The QMC model predicts three bound states for the charm-hypernucleus $^{16}_{\Lambda_c^+}\text{O}$. The predicted quantum numbers and binding energies of these states are shown in Table 1. We assume the initial bound proton state to have quantum numbers of the outermost $0p_{1/2}$ proton orbit of the target nucleus. The predicted binding energy of this state

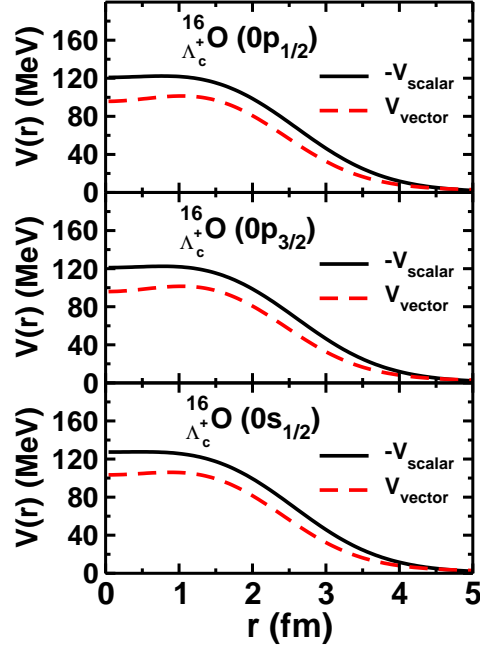


Figure 2: (color online) Vector and scalar potential fields felt by Λ_c^+ for $0p_{1/2}$, $0p_{3/2}$ and $0s_{1/2}$ Λ_c^+ states in $^{16}_{\Lambda_c^+}\text{O}$, where the vector potential field strength contains the effective Pauli blocking potential for each state of Λ_c^+ [see Eq. (17)].

by QMC is also shown in Table 1. The hypernuclear spectrum is clearly divided into three groups corresponding to the configurations $(0p_{1/2}^{-p}, 0s_{1/2}^{\Lambda_c^+})$, $(0p_{1/2}^{-p}, 0p_{1/2}^{\Lambda_c^+})$, and $(0p_{1/2}^{-p}, 0p_{3/2}^{\Lambda_c^+})$. Since $0p_{3/2}$ proton hole state has a much larger binding energy, any configuration mixing is expected to be negligible and has not been considered in this study.

In Fig. 2, we show the scalar and vector fields as calculated within the QMC model for $0p_{1/2}$, $0p_{3/2}$ and $0s_{1/2}$ Λ_c^+ states, where the strength of the vector field contains also the effective Pauli blocking potential for each state of Λ_c^+ (see Eq. (17)). It may be recalled that in the QMC model the scalar and vector fields are generated by the couplings of the σ and ω mesons to the quarks. Due to the different masses of these mesons and their couplings, especially the density dependence or non-linear dependence of the σN and $\sigma \Lambda_c^+$ coupling strengths due to the baryon internal structure, the scalar and vector fields may acquire non-trivial radial dependence. This is in contrast

to a phenomenological model where scalar and vector fields have the same Woods-Saxon (WS) radial form (see, e.g., Ref. [20]). In any case, because in such models the depths of these fields are searched to reproduce the experimental binding energies of a given state, they can not be applied at this stage to Λ_c^+ bound states due lack of any experimental information about them. In Fig. 2, we note that sum of the scalar and vectors fields at $r = 0$ is about -30 MeV for all the three states. This is roughly equivalent to the depth of a non-relativistic potential at this point. This is about 15 MeV less (in absolute value) than the depth of the Λ_c^+ - ^{16}O Hartree potential calculated in Ref. [23]. Therefore, relativistic self-consistent procedure has its consequences.

Figs. 3(a) and 3(b) show the moduli of the upper and lower components of $0p_{1/2}$, $0p_{3/2}$ and $0s_{1/2}$ Λ_c^+ spinors for the ^{16}O charm-hypernucleus in coordinate space and momentum space, respectively. The spinors in the momentum space are obtained by Fourier transformation of the corresponding coordinate space spinors. We note that only for $K_{\Lambda_c^+} < \text{approximately } 1.0 \text{ fm}^{-1}$, are the magnitudes of the lower components ($|g(K_{\Lambda_c^+})|$) substantially smaller than those of the upper components ($|f(K_{\Lambda_c^+})|$). In the region of $K_{\Lambda_c^+}$ pertinent to the charm-hypernuclear production, $|g(K_{\Lambda_c^+})|$ may not be negligible.

To get the T -matrix of the reaction of the process shown in Fig. 1(a), one has to integrate the amplitudes corresponding to each meson-exchange graph over the independent intermediate momenta k_p and $k_{\Lambda_c^+}$ subject to the constraints imposed by the momentum conservation at each vertex.

We have used plane waves to describe the motions of the \bar{p} and $\bar{\Lambda}_c^-$ baryon in the entrance and outgoing channels, respectively. However, initial- and final-state interactions are approximately accounted for within an eikonal-approximation based procedure [35] that was used in Refs. [10] to describe the charm-meson production in the \bar{p} -nucleus reactions. In this work we have employed the same parameters as those of Ref. [10] to estimate the distortion effects in the initial and final channels.

The threshold momentum for the production of $^{16}_{\Lambda_c^+}\text{O}$ in \bar{p} induced reaction on ^{16}O is about 3.953 GeV/c, while that for the $\bar{\Lambda}_c^- + \Lambda_c^+$ production in the elementary $\bar{p} + p$ reaction is 10.162 GeV/c. The shift in the threshold of the hypernuclear production reaction to lower beam momenta is mainly due to the Fermi motion effects. Therefore, Λ_c^+ hypernuclear production experiments may be feasible even in the beginning stage of the FAIR project when \bar{p} beam momenta may be lower than their maximum planned value of

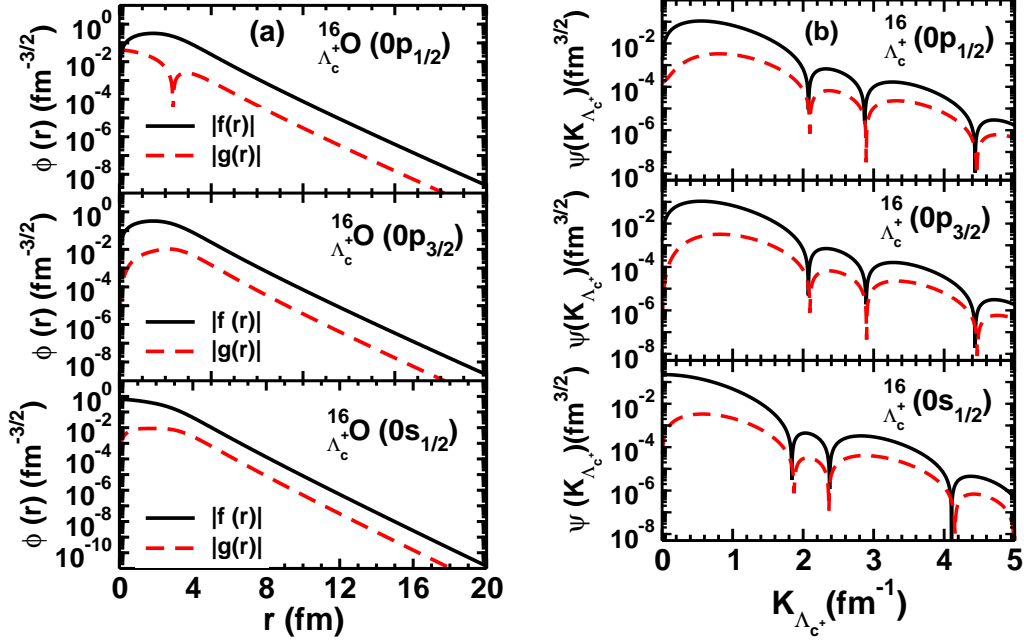


Figure 3: (color online) (a) Moduli of the upper ($|f(r)|$) and lower ($|g(r)|$) components of the coordinate space spinors for $0p_{1/2}$, $0p_{3/2}$ and $0s_{1/2}$ Λ_c^+ states in $^{16}_{\Lambda_c^+}\text{O}$. Solid lines represent the upper component while the dashed line the lower component. (b) Moduli of upper (solid lines) and lower (dashed lines) components of the momentum space spinors of the Λ_c^+ bound states in $^{16}_{\Lambda_c^+}\text{O}$ for the same states as in the left panel.

15 GeV/c.

In Fig. 4, we show the 0° differential cross sections $[(d\sigma/d\Omega)_0]$ for the reaction $\bar{p} + ^{16}\text{O} \rightarrow \bar{\Lambda}_c^- + ^{16}_{\Lambda_c^+}\text{O}$ obtained by using the proton-hole and Λ_c^+ bound state spinors calculated within the QMC model. Cross sections are shown for \bar{p} beam momenta in the range of threshold to 20 GeV/c. The charm-hypernuclear states populated are 1^- and 0^- , 1^+ and 0^+ , and 2^+ and 1^+ corresponding to the particle-hole configurations $(0p_{1/2}^{-p}, 0s_{1/2}^{\Lambda_c^+})$, $(0p_{1/2}^{-p}, 0p_{1/2}^{\Lambda_c^+})$, and $(0p_{1/2}^{-p}, 0p_{3/2}^{\Lambda_c^+})$, respectively. Cross sections to the higher J state of each configuration are shown in Fig. 4(a), while those to lower J in Fig. 4(b). We see that for each particle-hole configuration, the state with higher J has larger cross section. While for beam momenta ≥ 8 GeV/c, the cross-sections for states belonging to the $(0p_{1/2}^{-p}, 0s_{1/2}^{\Lambda_c^+})$ configuration are larger than those of the other two configurations, for $p_{\bar{p}}$ lower than 8 GeV/c those for states

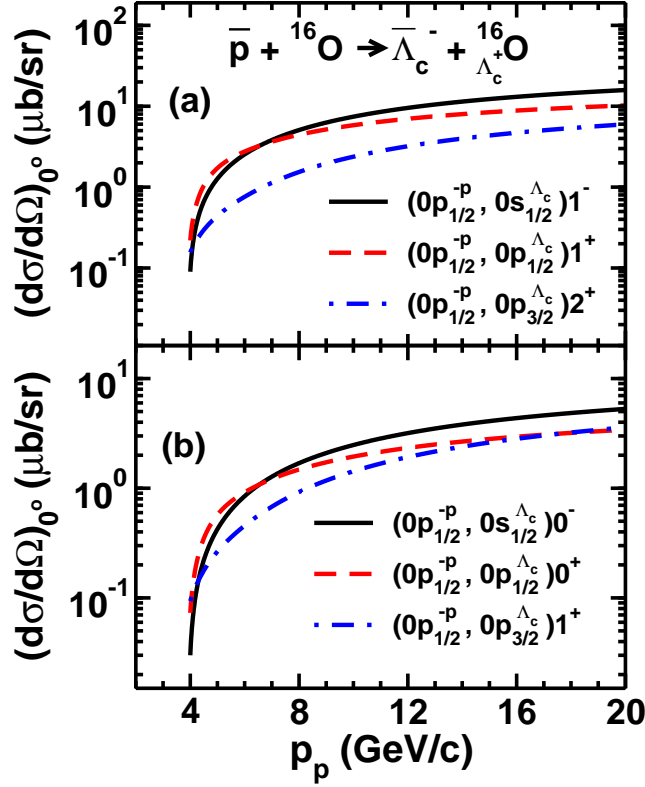


Figure 4: (color online) (a) Differential cross sections at 0° of the $\bar{p} + {}^{16}\text{O} \rightarrow \bar{\Lambda}_c^- + {}^{16}_{\Lambda_c^+}\text{O}$ reaction leading to the ${}^{16}_{\Lambda_c^+}\text{O}$ hypernuclear states of larger J value of each particle-hole configuration as indicated. (b) The same as in (a) but for states of lower J value of each configuration as indicated. In the legends Λ_c corresponds to Λ_c^+ .

belonging to the $(0p_{1/2}^{-p}, 0p_{1/2}^{+\Lambda_c})$ configuration have larger values. However, the maximum difference between the cross sections of the states belonging to two configurations is not more than a factor of 1.4. The $[(d\sigma/d\Omega)_0]$, for the states belonging to the configuration $(0p_{1/2}^{-p}, 0p_{3/2}^{+\Lambda_c})$ are smaller than those of the $(0p_{1/2}^{-p}, 0p_{1/2}^{+\Lambda_c})$ configuration by factors of approximately 1.4 - 3.0.

It is to be noted that for \bar{p} beam momenta between 8 - 15 GeV/c (which are of interest to $\bar{P}ANDA$ experiment) the magnitudes of the 0° differential cross sections vary between 1.5 - 3.8 $\mu\text{b/sr}$, and 5.0 - 11.0 $\mu\text{b/sr}$ for states 0^- and 1^- , respectively, of the configuration $(0p_{1/2}^{-p}, 0s_{1/2}^{+\Lambda_c})$. On the other hand,

for states 1^+ and 2^+ of the configuration $(0p_{1/2}^{-p}, 0p_{3/2}^{\Lambda_c^+})$, it varies between 0.9 - 2.8 $\mu\text{b/sr}$, and 1.6 - 6.0 $\mu\text{b/sr}$, respectively. Furthermore, the cross sections for all the states consist almost solely of the contributions from the D^{*0} meson-exchange process, with D^0 meson-exchange terms being very small. This is similar to what has been noted in the case of the elementary $\bar{p}+p \rightarrow \bar{\Lambda}_c^- + \Lambda_c^+$ reaction in Ref. [6]. The domination of the D^{*0} exchange process has been traced to the strong tensor coupling term of the D^{*0} meson couplings.

We next discuss the uncertainties and the range of validity of our results. We use an eikonal-approximation based phenomenological method to account for the initial- and final-state interaction effects. In the recent past [12, 54], similar methods have been used for this purpose in other studies also where models like ours have been employed to investigate the hypernuclear productions of different types in the \bar{p} -nucleus collisions. However, due to lack of the adequate experimental information on the elastic scattering data these methods involve parameters, which may not be properly constrained. This constitutes a major source of uncertainty in such calculations.

Our procedure [10] involves basically two parameters; namely, the \bar{p} -nucleon and $\bar{\Lambda}_c^-$ -nucleon total cross sections ($\sigma_{\bar{p}N}$, and $\sigma_{\bar{\Lambda}_c^-N}$, respectively). Out of these $\sigma_{\bar{p}N}$ is of crucial importance. Its value has been quoted to be some where between 50 mb and 81 mb for \bar{p} momenta above 2 GeV/c (see, Refs. [55, 56, 57]). The results shown in Figs. 4(a) and 4(b) have been obtained with a $\sigma_{\bar{p}N}$ of 75 mb. Nevertheless, we have also performed calculations by using $\sigma_{\bar{p}N}$ of 50 mb and 81 mb in order to access the uncertainty in the magnitudes of our cross sections. For the $(0p_{1/2}^{-p}, 0p_{1/2}^{\Lambda_c^+})$ configuration, at the \bar{p} beam momentum of 15 GeV/c, the cross sections increase by factor of almost 2 or decrease by about 10% by using $\sigma_{\bar{p}N} = 50$ mb and 81 mb, respectively, as compared to those obtained with $\sigma_{\bar{p}N} = 75$ mb. Thus, there could to be an uncertainty of a factor of up to 2 in our cross sections on this account. Furthermore, our method necessarily assumes that the shapes of the angular distributions are not influenced by the distortion effects. This may change in a more rigorous treatment of distortions that includes both absorption and dispersion effects.

Results of the calculations performed within our model are also sensitively dependent on the values of the coupling constants at various vertices involved in the t -channel diagrams, and on the shape of the form factor and the value of the cutoff parameter λ_i .

As stated earlier, the coupling constants at the vertices involved in the

t -channel diagrams, have been adopted from Refs. [47, 49, 50], where they have been fixed by using the SU(4) symmetry arguments in the description of the exclusive charmed hadron production in the $\bar{D}N$ and DN scattering within a one-boson-exchange picture. While, we acknowledge that the SU(4) symmetry will not hold rigorously, the level of deviations from the SU(4) coupling constants in the charm sector has been reported to be highly model dependent [58]. Recent calculations within light-cone sum rules suggest that deviations from the SU(4) values of the relevant coupling constants are limited to factors of 2 or less [59]. On the other hand, in constituent quark model calculations using the 3P_0 quark-pair creation mechanism, the deviations are at the most of the order of 30% [60].

There may indeed be some uncertainty in our cross sections coming from the shape of the form factor and the value of the cutoff parameter (λ_i) involved therein. We have employed a monopole form factor with a λ_i of 3.0 GeV. Obviously, a form factor of a different shape and/or a different value of λ_i would lead to a different cross section. We have tried to minimize such uncertainties in our cross sections by using the same shape (monopole) of the form factor and the same value of λ_i (3.0 GeV) that were used in our previous study of the free-space charmed baryon production in the $\bar{p}p$ collisions [6]. The same form factor with the same cutoff parameter were also used in the calculations of the charm baryon production cross sections within the Jülich meson-exchange model [8]. Moreover, this ansatz for the form factor and the value of the cutoff parameter λ_i have been checked by fitting the data on the $pp \rightarrow \Lambda_c^+ X$ reaction measured by the ISR Collaboration in Ref. [48].

In summary, we have studied the 0° differential cross sections for the production of the charm-hypernucleus $^{16}_{\Lambda_c^+}\text{O}$ in the antiproton - ^{16}O collisions within a covariant model. In our calculations, $\bar{\Lambda}_c^- \Lambda_c^+$ production takes place via the t -channel exchanges of D^0 and D^{*0} mesons in the initial collisions of the \bar{p} with a target proton. Λ_c^+ gets captured into one of the nuclear orbits while $\bar{\Lambda}_c^-$ goes out. Λ_c^+ bound state spinors are derived from the quark-meson coupling model. The coupling constants at the meson exchange vertices are taken to be the same as those used in a previous study of the elementary $\bar{p} + p \rightarrow \bar{\Lambda}_c^- + \Lambda_c^+$ reaction by one of us [6]. The off-shell corrections at the vertices are accounted for by introducing monopole form factors with a cut-off parameter of 3.0 GeV, which is the same as that used in Ref. [6].

At beam momenta of interest to the $\bar{P}ANDA$ experiment, the 0° differential cross section for the $\bar{p} + ^{16}\text{O} \rightarrow \bar{\Lambda}_c^- + ^{16}_{\Lambda_c^+}\text{O}$ reaction varies between 0.9

$\mu\text{b/sr}$ to $11 \mu\text{b/sr}$ depending on the final Λ_c^+ state excited in the reaction. The relatively larger cross sections and low threshold for the production of the $^{16}_{\Lambda_c^+}\text{O}$ hypernuclear states in the $\bar{p} - ^{16}\text{O}$ reaction may make it possible to perform such experiments at the $\bar{P}ANDA$ facility even in the beginning stage of the FAIR.

We acknowledge that there are uncertainties in our cross sections due to the imprecise knowledge of the parameters involved in the treatment of initial- and final-state interaction effects. We provided estimates of these uncertainties. Accumulation of the precise relevant data by the $\bar{P}ANDA$ experiment at the FAIR facility will help in having a better understanding of these effects.

This work has been supported by the Science and Engineering Research Board (SERB), Department of Science and Technology, Government of India under Grant no. SB/S2/HEP-024/2013, and by Fundação de Amparo à Pesquisa do Estado de São Paulo (FAPESP), Brazil, Grants No. 2016/04191-3, and, No. 2015/17234-0, and Conselho Nacional de Desenvolvimento Científico e Tecnológico (CNPq), Grants No. 400826/2014-3 and No. 308088/2015-8.

References

- [1] M. Neubert, Phys. Rep. **245** (1994) 259.
- [2] J. G. Körner, M. Krämer, and D. Pirjol, Prog. Part. Nucl. Phys. **33** (1994) 787.
- [3] W. Erni *et al.*, arXiv:0903.3905 [hep-ex].
- [4] U. Wiedner, Prog. Part. Nucl. Phys. **66** (2011) 477
- [5] E. Prencipe, Eur. Phys. J. Web. Conf. **95** (2015) 04052.
- [6] R. Shyam and H. Lenske, Phys. Rev. D **90** (2014) 014017.
- [7] R. Shyam and H. Lenske, Phys. Rev. D **93** (2016) 034016.
- [8] J. Haidenbauer, and G. Krein, Phys. Lett. B **678** (2010) 314.
- [9] J. Haidenbauer, and G. Krein, Phys. Rev. D **89**, (2014) 114003.
- [10] R. Shyam and K. Tsushima, Phys. Rev. D. **94** (2016) 074041.

- [11] A. Hosaka, T. Hyodo, K. Sudoh, Y. Yamaguchi and S. Yasui, arXiv:1606.08685 [hep-ph]
- [12] J. Yamagata-sekihara, C. Garcia-Recio, J. Nieves, L. L. Salcedo, and L. Tolos, Phys. Lett. **B 754** (2016) 26.
- [13] S. K. Choi et al. (Belle Collaboration), Phys. Rev. Lett. **91** (2003) 262001.
- [14] S. K. Choi et al. (Belle Collaboration), Phys. Rev. Lett. **100** (2008) 142001.
- [15] S. Godfrey and S. L. Olsen, Ann. Rev. Nucl. Part. Sci. **58** (2008) 51.
- [16] T. Miyamoto (for HAL QCD collaboration), arXiv:1602.07797 [hep-lat]
- [17] O. Hasimoto and H. Tamura, Prog. Part. Nucl. Phys. **57** (2006) 564.
- [18] R. Shyam, Prog. Part. Nucl. Phys. **61** (2008) 212.
- [19] A. Gal, E.V. Hungerford and D.J. Millener, Rev. Mod. Phys. **88** (2016) 035004.
- [20] R. Shyam, K. Tsushima, and A. W. Thomas, Nucl. Phys. **A881** (2012) 255.
- [21] A. A. Tyapkin, Sov. J. Nucl. Phys. **22** (1975) 181.
- [22] S. Iwato, Lett. Nuovo Cim. **19** (1977) 647.
- [23] C. B. Dover and S. H. Kahana, Phys. Rev. Lett. **39** (1977) 1506.
- [24] R. Gatto and F. Paccanoni, Nuovo Cim. **A46** (1978) 313.
- [25] N. N. Kolesnikov et al., Sov. J. Nucl. Phys. **34** (1981) 533.
- [26] G. Bhamathi, Phys. Rev. C **24** (1981) 1816.
- [27] H. Bando and M. Bando, Phys. Lett. **B109** (1982) 164.
- [28] B. F. Gibson, C. B. Dover, G. Bhamathi, and D. R. Lehman, Phys. Rev. C **27** (1983) 2085.
- [29] C. H. Cai, L. Li, Y. H. Tan, P. Z. Ning, Europhys. Lett. **64** (2003) 448.

- [30] K. Tsushima and F. C. Khanna, Phys. Lett. **B552** (2003) 138.
- [31] K. Tsushima and F. C. Khanna, Phys. Rev. C **67** (2003) 015211.
- [32] K. Tsushima and F. C. Khanna, Prog. Theo. Phys. Suppl. **149** (2003) 149.
- [33] K. Tsushima and F. C. Khanna, J. Phys. G: Nucl. Part. Phys. **30** (2004) 1765.
- [34] R. Shyam, H. Lenske and U. Mosel, Phys. Rev. C **69** (2004) 065205.
- [35] R. Shyam, H. Lenske and U. Mosel, Nucl. Phys. **A764** (2006) 313.
- [36] R. Shyam, K. Tsushima and A. W. Thomas, Phys. Lett. **B676** (2009) 51.
- [37] S. Bender, R. Shyam and H. Lenske, Nucl. Phys. **A 839** (2010) 51.
- [38] J. Haidenbauer and G. Krein, Phys. Rev. D **95** (2017) 014017.
- [39] P. A. M. Guichon, Phys. Lett. **B200** (1988) 235.
- [40] B. D. Serot and J. D. Walecka, Adv. Nucl. Phys. **16** (1986) 1; *ibid*, Int. J. Mod. Phys. **E 6** (1997) 515.
- [41] K. Saito, K. Tsushima and A. W. Thomas, Nucl. Phys. **A609** (1996) 339.
- [42] K. Tsushima, D. H. Lu, A. W. Thomas, and K. Saito, Phys. Lett. **B443** (1998) 26.
- [43] K. Tsushima, K. Saito, J. Haidenbauer and A. W. Thomas, Nucl. Phys. **A630** (1998) 691.
- [44] K. Tsushima, D. H. Lu, A. W. Thomas, K. Saito R. H. Landau, Phys. Rev. C **59** (1999) 2824.
- [45] K. Saito, K. Tsushima and A. W. Thomas, Prog. Part. Nucl. Phys. **58** (2007) 1.
- [46] A. Müller-Groeling, K. Holinde, and J. Speth, Nucl. Phys. **A513** (1990) 557.

- [47] J. Haidenbauer, G. Krein, U.-G. Meissner, and L. Tolos, Eur. Phys. J. A **47** (2011) 18.
- [48] T. J. Hobbs, J. T. Londergan, and W. Melnitchouk, Phys. Rev. D **89** (2014) 074008.
- [49] J. Haidenbauer, G. Krein, U.-G. Meissner, and A. Sibirtsev, Eur. Phys. J. A **33** (2007) 107.
- [50] J. Haidenbauer, G. Krein, U.-G. Meissner, and A. Sibirtsev, Eur. Phys. J. A **37** (2008) 55.
- [51] R. Shyam, Phys. Rev. C **60** (1999) 055213.
- [52] R. Shyam and U. Mosel, Phys. Rev. C **67** (2003) 065202.
- [53] K. A. Olive *et al.* (Particle Data Group), Chin. Phys. C **38** (2014) 090001.
- [54] A. B. Larionov and H. Lenske, arXiv:1703.02073 [nucl-th].
- [55] A. B. Larionov and H. Lenske, Nucl. Phys. **A957** (2017) 450.
- [56] Teck-Ghee Lee and Cheuk-Yin Wong, Phys. Rev. C **89** (2014) 054601.
- [57] Zhang Yu-shun, Liu Ji-feng, B. A. Robson, and Li Yang-guo, Phys. Rev. C **54** (1996) 332.
- [58] G. Krein, POS (Confinement X) (2012) 144.
- [59] A. Khodjamirian, C. Klein, T. Mannel, and Y. M. Wang, Eur. Phys. J. A **48** (2012) 23.
- [60] G. Krein, EPJ Web Conf. **73** (2014) 05001.